Arch. Metall. Mater. **68** (2023), 3, 907-919

DOI: https://doi.org/10.24425/amm.2023.145454

LI HUI[1], SUN CAIZHI[1], WANG FENG[1], QIAO YUANPENG[1], LI CHUYING[1],
XU PINYI[1], ANDRII ZATULOVSKIY[2], VOLODYMYR SHCHERETSKYI[2]

STUDY ON MICROSTRUCTURE AND MECHANICAL PROPERTIES OF FRICTION STIR WELDING JOINTS OF IN-SITU Al_3Zr/AA6082 PARTICLE-REINFORCED ALUMINUM MATRIX COMPOSITES

In this paper, the Al-K_2ZrF_6 reaction system was used to prepare in-situ Al_3Zr/AA6082 particle-reinforced aluminum matrix composites by electromagnetic stirring melt reaction method, and the friction stir welding technology was used to weld the plate. The microstructure and mechanical properties of the welded joints were studied when the rotating speed was 14000 rpm and the welding speed was 30, 50 and 70 mm/min respectively. The results show that the weld forming quality and tensile properties of the FSW joints with welding parameters of 14000 rpm and 50 mm/min are the best, the tensile strength is 142(±0.5) MPa and the elongation is 8.2%. SEM analysis shows that the particle size of the reinforcing phase in the base metal is refined to about 5-10 μm, while that in the NZ is about 1-5 μm. The grain size in the HAZ is about 20-30 μm and in the NZ is about 5-10 μm. EBSD analysis shows that the proportion of low-angle grain boundary in the NZ is 59.7% and of recrystallized grain structure is 23.65%, while the proportion of small-angle grain boundary in the HAZ is 24.35% and of recrystallized grain structure is 37.18%. It provides theoretical and experimental basis for the forming and application of friction stir welding of the composite.

Keywords: aluminum matrix composite; in-situ; FSW; microstructure; mechanical properties

1. Introduction

Aluminum matrix composites have good conductivity and corrosion resistance, high specific modulus and specific strength, which are often used as structural materials for aerospace, high-speed rail and automotive industries with great demand for lightweight materials [1-8]. The melting point, thermal conductivity and linear expansion coefficient of the reinforced phase in the composites are greatly different from those of the matrix aluminum alloy, which makes the welding performance of the aluminum matrix composites very poor and the weld is easy to form holes and inclusions.

Friction Stir Welding (FSW) is a solid-state joining technology. Compared with the traditional melting welding technology, friction stir welding has quieter working environment, lower pollution and lower energy consumption [9-15]. Due to the low welding heat input, friction stir welding can reduce the welding residual stress and post-welding deformation, improve the compactness of the weld microstructure and avoid the loss of stirring head [16-23]. Friction stir welding is widely used in aluminum matrix composites with poor welding performance due to the advantages of low welding heat input and no molten pool that traditional fusion welding does not have [24-29]. Friction stir welding joints can often be divided into three regions: nugget zone (NZ), thermo-mechanically affected zone (TMAZ) and heat affected zone (HAZ). Jingyi Zhang et al. [30] analyzed the microstructure of friction stir welding AA7075-T6 billet at welding speeds of 1, 2 and 3 m/min. The analysis shows that the higher the welding speed, the narrower and stronger the heat affected zone, and the higher the hardness of the nugget zone. With the increase of welding speed, the material flow direction in NZ tends to the welding direction. The combination of the results with the welding parameters and thermal history helps to understand the complex material flow and texture gradient in the weld, so as to optimize the welding parameters of high-speed machining. Chong Gao et al. [31] welded 1.8 mm 2198-T8 aluminum-lithium alloy cold-rolled sheet at speed of 800 rpm and at welding speed of 300 mm/min by friction stir welding. During FSW, the grains in HAZ become coarse, while the fine equiaxed grains are 4.6-6.2 μm. A large number of T1 phase dispersed in the weld metal and gradually dissolved when close to the weld center. The hardness distribution of FSW joint is like a 'basin'.

[1] JIANGSU UNIVERSITY OF SCIENCE AND TECHNOLOGY, SCHOOL OF MATERIALS SCIENCE AND ENGINEERING, ZHENJIANG 212000, CHINA
[2] PHISICO-TECHNOLOGICAL INSTITUTE OF METALS AND ALLOYS OF THE NATIONAL ACADEMY OF SCIENS OF UKRAINE, KYIV, UKRAINE

* Corresponding author: lihuiwind@163.com

The maximum hardness of 180 $HV_{0.2}$ is located in BM, while the minimum hardness (90 $HV_{0.2}$) is obtained in the weld center area. The hardness distribution is closely related to the evolution of precipitates. After FSW, due to the dissolution of precipitates, the strength of FSW 2198 joints in different regions decreased compared with BM. The analysis shows that the strengthening mechanisms in BM, HAZ and TMAZ are mainly dislocation and precipitation hardening, while in the stir shoulder zone (SsZ) and stir pin zone (SpZ) are dislocation hardening and grain refinement strengthening. C. Yang et al. [32] welded 6082Al alloy plate with 80 mm thickness on both sides by FSW. The relationship between microstructure and mechanical properties was established, and the local microstructure and mechanical properties were studied in detail. The tensile properties of the whole joint were tested by three slice specimens. Similar UTS of 230 MPa, 225 MPa and 223 MPa were obtained by secondary welding, interlayer and primary welding, respectively, which reached 70% of BM.

The above research shows that the mechanical properties and micro-corrosion properties of friction stir welded joints of aluminum matrix composites have great research value. In this paper, the friction stir welding technology was used to test the 2 mm aluminum matrix composite plate. The ultra-high rotating speed friction stir welding with the rotational speed of 14000 rpm was used to study the influence of welding speed on the microstructure of the joints and the morphology and distribution of the reinforcement particles. The effects of different grain sizes and morphology and distribution of reinforcements in weld zone on microhardness and tensile properties were studied. EBSD technology was used to characterize the grain morphology, grain boundary orientation difference and microstructure deformation characteristics of FSW joints in different regions.

2. Materials and methods

In this experiment, Al_3Zr/AA6082 particulate-reinforced aluminum matrix composites were prepared by melt reaction method with electromagnetic stirring. Al_3Zr content is 3.5wt%. The matrix of aluminum matrix composites is AA6082 aluminum alloy, and the reaction salt is K_2ZrF_6. The matrix alloy composition is shown in TABLE 1.

TABLE 1

Chemical composition of Aluminum matrix (wt%)

Si	Fe	Cu	Mn	Mg	Ni	Zn	Al
1.09	0.218	0.552	0.231	2.40	0.25	2.01	Bal.

The composite was cut into 10×4×2 mm plate and cleaned with ethanol and acetone. The welding test equipment in this paper is an ultra-high rotating speed friction stir welding machine independently developed and assembled by our school. The rotating speed range is 6000-15000 r/min, and the spindle power is 7.5 KW. The equipment is shown in Fig. 1. The stirring head used in the friction stir welding of 2 mm plate was the Tool-10-2 stirring head of Beijing Saifuster Co., Ltd., whose stirring pin was designed as a round table. The stirring head is made of H13 die steel. The diameter of the stirring shaft shoulder was 10 mm, the length of the pin was 1.90 mm, and the diameter of the tip of the stirring pin was 3.2 mm. The shape of the stirring pin is shown in Fig. 2. The stirring head would rotate clockwise with an inclination of 2°. The rotating speed was fixed at 14000 rpm, and the welding speeds were 30, 50 and 70 mm/min, respectively. The part perpendicular to the welding direction of joints after welding were taken as observation objects. Metallographic samples were corroded with 5% hydrofluoric acid for 2 min.

Optical microscope (Axio Observer; Zeiss, Germany) was used to observe the morphology and structure of the weld zone interface. Scanning electron microscope (SEM) (Merlin Compact; Zeiss) was used to study the solidification structure, morphology, particle size and distribution of the reinforcement phase. The reinforcement phase content was evaluated by energy dispersive spectrometer (EDS) (Merlin Compact; Zeiss). Using the above scanning and transmission electron microscopy (JEM-2100F; JEOL, Japan) to observe and analyze the microstructure of the joints. The samples were prepared by mechanical dilution method and electrolytic double jet dilution method (25 ml $HClO_4$ + 475 ml C_2H_5OH). The cross sections of FSW joints were

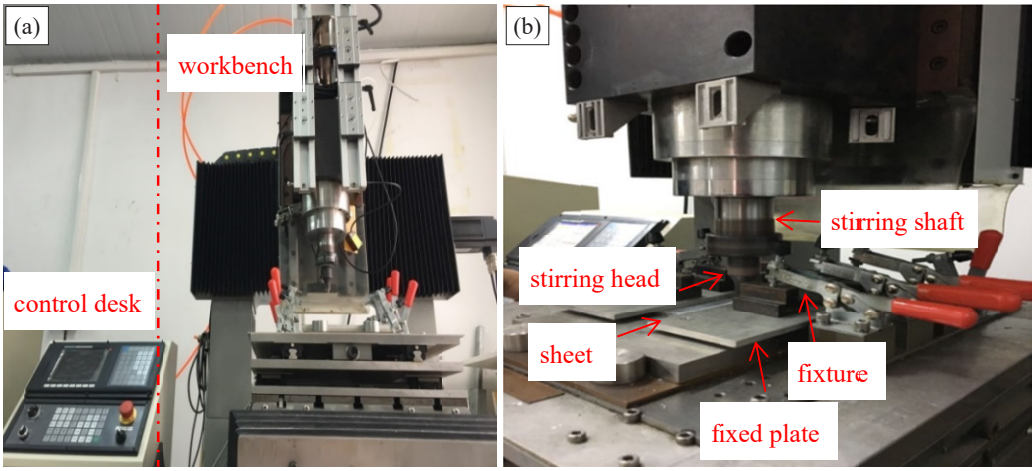

Fig. 1. Friction Stir Welding equipment. (a) New high-speed friction stir welding equipment; (b) Equipment workbench and its specific parts

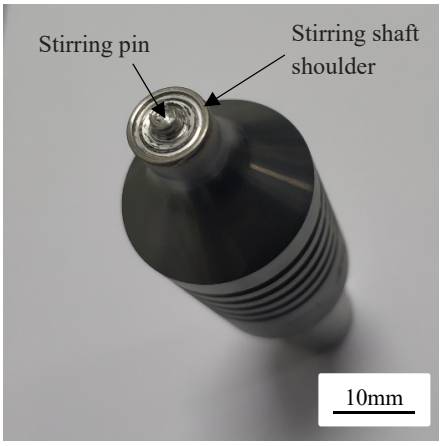

Fig. 2. FSW tools for friction stir welding

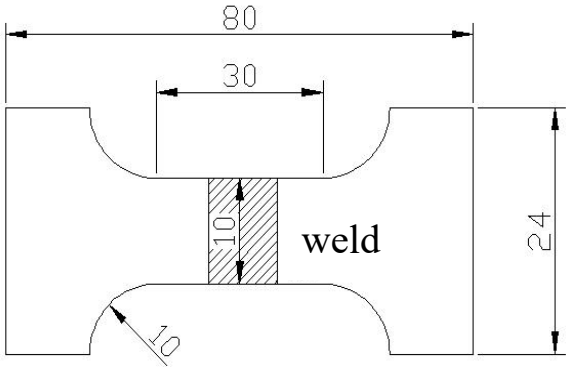

Fig. 3. Schematic diagram of tensile specimen size

cut and polished, and the microhardness was tested by taking 20 points in each of three straight lines, respectively 0.5 mm, 1.0 mm and 1.5 mm away from the upper surface of the weld, with an interval of 0.5 mm. The starting and ending points are 5 mm on either side of the weld center, respectively. The load is selected as $HV_{0.2}$. The tensile specimens of 2 mm sheet and welded joints were cut. The total length of the specimens was 80 mm, the parallel length was 30 mm, the width was 10 mm, and the tensile rate was 1 mm/min. The dimensions of the tensile specimen are shown schematically in Fig. 3.

3. Results and Discussion

3.1. Microstructure of matrix composite

The tissue morphology of the composites was observed by scanning electron microscopy and the elemental distribution was analyzed by EDS. The microstructure of the aluminum matrix composites is shown in Fig. 4. From Fig. 4(a-b), it can be seen that the light white reinforcing phase particles are distributed on the dark alloy matrix. The reinforcing phase particles of the composite are uniformly distributed, and the particle morphology is mainly massive, rectangular and a very small amount of needle shape, and the particle size is 5-10 μm. The particle size is within the best range of the study [33]. From the composition point scan of the reinforcing phase particles, it can be seen that the point composition is mainly Al and Zr, and combined with the XRD physical phase analysis results, it is known that the second phase particles in the matrix are the reinforcing phase Al_3Zr.

The element distribution of the aluminum matrix composites is shown in Fig. 5(b-d), which shows that the Zr elements are concentrated in the location of the reinforcing phase particles, indicating that the second phase particles in the figure are Al_3Zr. Al and Mg elements are diffusely distributed throughout the domain, indicating that the matrix is a replacement solid solution of Mg and Al.

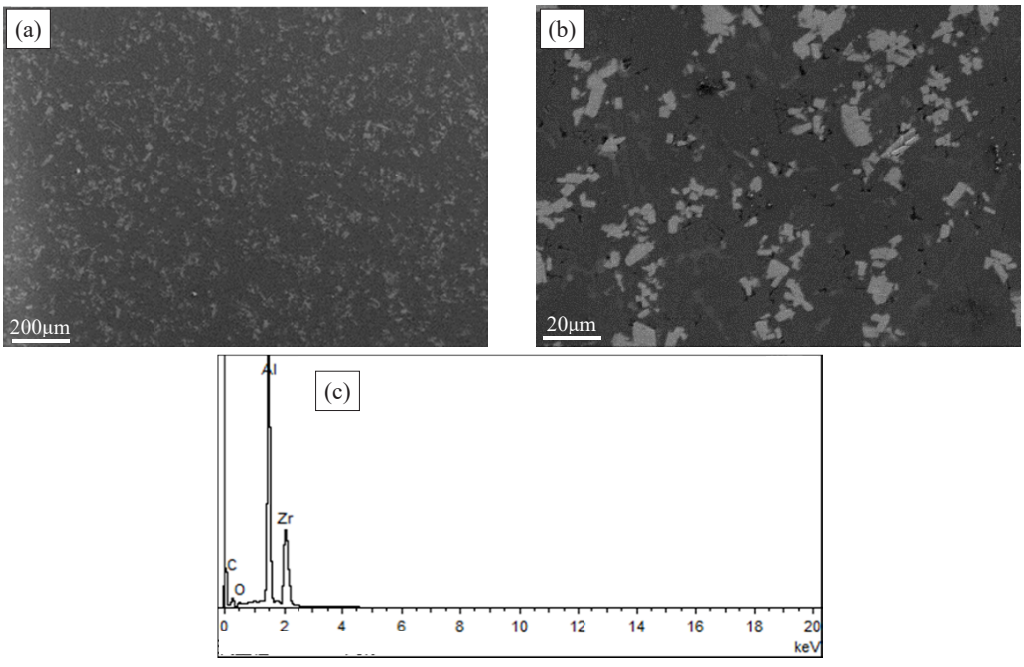

Fig. 4. Microstructure of Aluminum matrix composite. (a-b) SEM micrograph; (c) EDS map of Al_3Zr

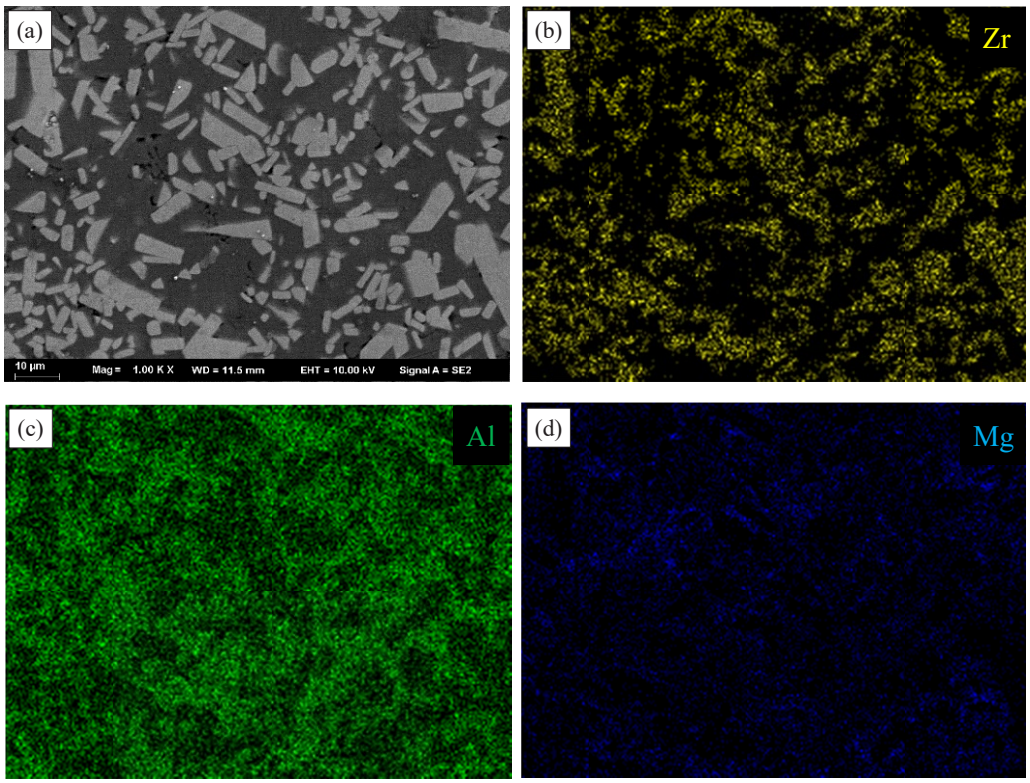

Fig. 5. Element distribution of microstructure of Aluminum matrix composite. (a) Microstructure; (b) Zr; (c) Al; (d) Mg

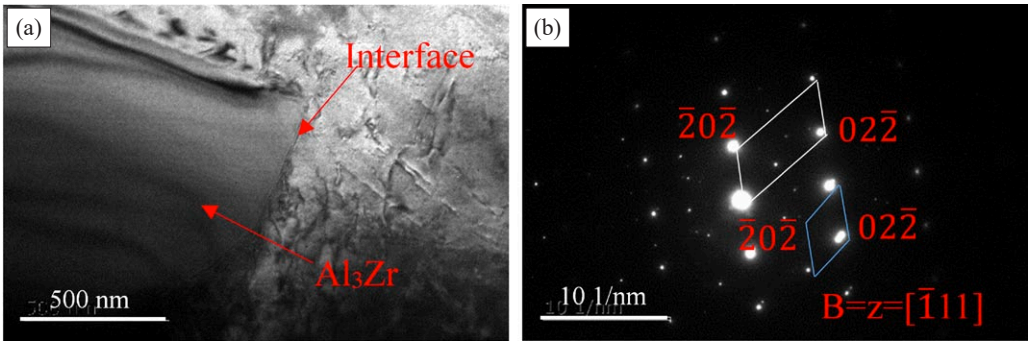

Fig. 6. (a) TEM micrograph of aluminum matrix composite; (b) Diffraction spot of aluminum matrix composite

Fig. 6 shows the microscopic morphology of the aluminum matrix composite by transmission electron microscopy. It can be seen from the figure that the reinforcing phases of the aluminum matrix composites are all blocky in shape with smooth edges, and the bonding interface with the matrix is clean and free of inclusions and voids. Fig. 6(b) shows the diffraction spot of Fig. 6(a), and the comparison of the diffraction spot of the matrix and the reinforced phase shows that both of them have the same crystallographic index [$\bar{1}$11], which indicates that the matrix and the reinforced phase particles have a certain crystal lattice at this crystallographic index, which laterally indicates that the in situ endogenous Al_3Zr reinforced phase particles are well bonded with the matrix metal. These results are in good agreement with references [34], the in situ endogenous Al_3Zr/AA6082 particle-reinforced aluminum matrix composites have the advantages of good wetting properties, clean interfacial bonding without defects and no interfacial reactions.

3.2. Effects of different welding speeds on weld surface forming

Fig. 7 shows the macroscopic morphology of FSW joints with different welding speeds. Fig. 7(a-b) shows the FSW joint with the speed of 30 mm/min. It can be seen from the figure that the weld surface of the joint is gray, and there are serious flashes on the edge, while the internal structure of the weld is dense, and there are no defects such as holes. Fig. 7(c-d) shows the FSW joint with the speed of 50 mm/min. It can be seen that the microstructure of the weld is relatively dense, without obvious defects, and the grains in the weld are smaller and more uniform than those in BM. Fig. 7(e-f) shows the FSW joint with the speed of 70 mm/min.

There are small holes on the weld surface of the joint and a lot of voids in the weld, which means that the material is not fully filled. This is because when the rotating speed is constant,

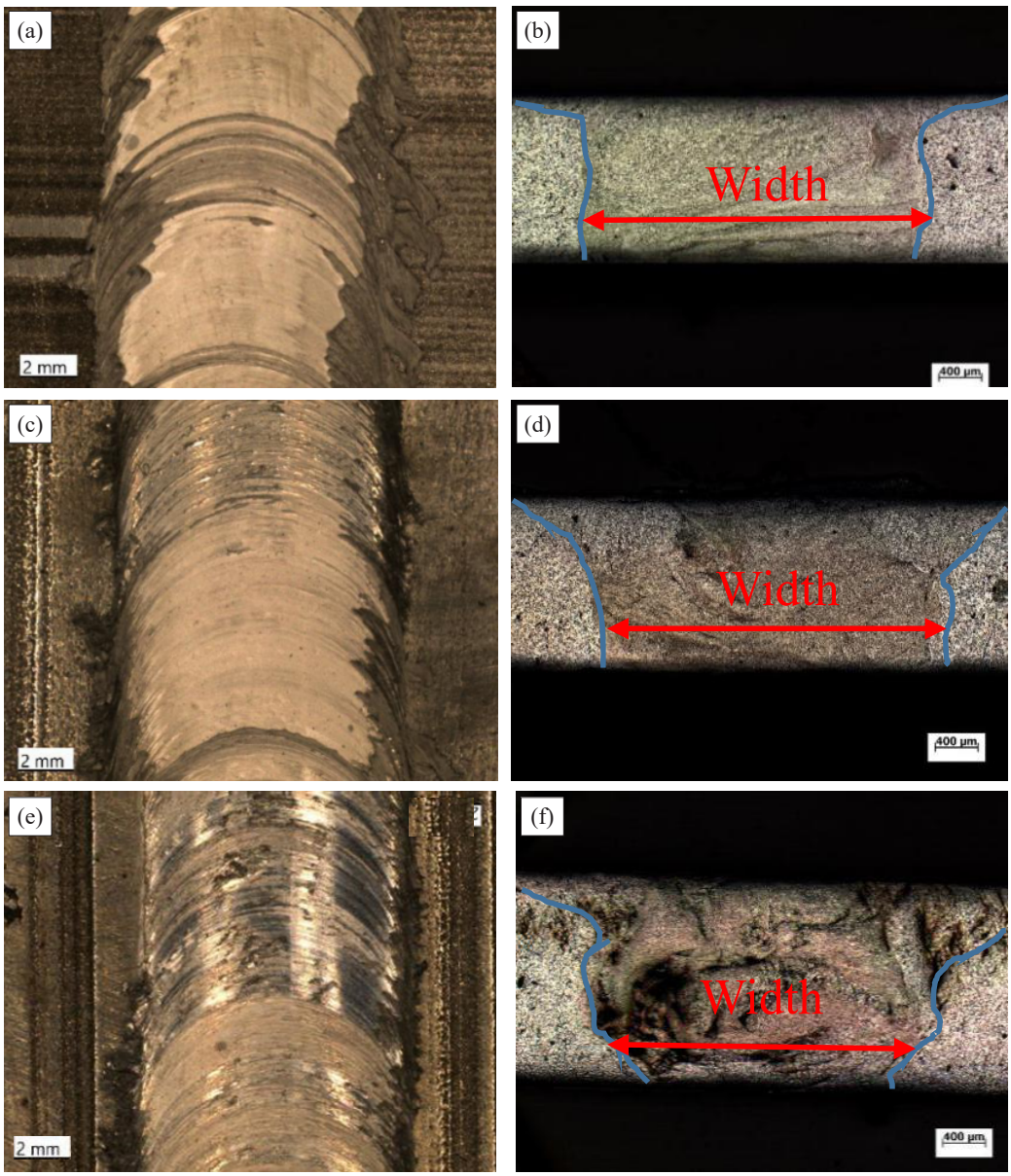

Fig. 7. Macro morphology of FSW joints with different travel speeds. (a-b) 14000 r/min, 30 mm/min; (c-d) 14000 r/min, 50 mm/min; (e-f) 14000 r/min, 70 mm/min

the heat generated by the friction between the stirring head and the material surface is fixed. When the welding speed is low, the heat accepted by the weld material in unit time is large, so the plasticizing degree of the weld material is high. The softened material is squeezed out of the weld bead, so the weld edge produces serious flashes and the surface is oxidized to discoloration. When the welding speed is high, the thermal cycle of the material at the weld is low, and the mechanical stirring effect of the stirring head is also weak, so the weld cannot be fully filled, and there are gaps and other defects. At the same time, by comparing the cross-section shapes of welds with different welding speeds, it can be seen that the weld width decreases with the increase of welding speed. When the welding speed is 30 mm/min, the weld cross-section shape is nearly rectangular; when the welding speed is 50 mm/min, the weld cross-section shape is inverted trapezoidal; and when the welding speed is 70 mm/min, the bottom width of the weld cross-section is further reduced. This is because with the increase of welding speed, the heat transferred from the stirring head to the weld decreases in unit time. Since the bottom of the weld is only subject to the friction heat caused by the rotation of the stirring pin, the higher the welding speed is, the less the heat input at the bottom of the weld is, and the width of the weld is also reduced. Recently in (2021) S. Rajkumar et al. [35] concluded similar results in case of friction stir welding of AA6061 Al alloy.

3.3. Phase analysis and microstructure evolution of FSW joints

In order to analyze whether the welding thermal cycle during friction stir welding causes the phase change in FSW joints, the FSW joints with different parameters were characterized

by X-ray diffractometer. Fig. 8 is the XRD patterns of friction stir welded joints. It can be seen from the figure that no new phase was generated in the FSW joints with various welding parameters. Meanwhile, the characteristic peak strength of the reinforcement, Al_3Zr, was lower than that of the raw material, which indicates that the reinforcement particles were broken into small particles during the stirring process.

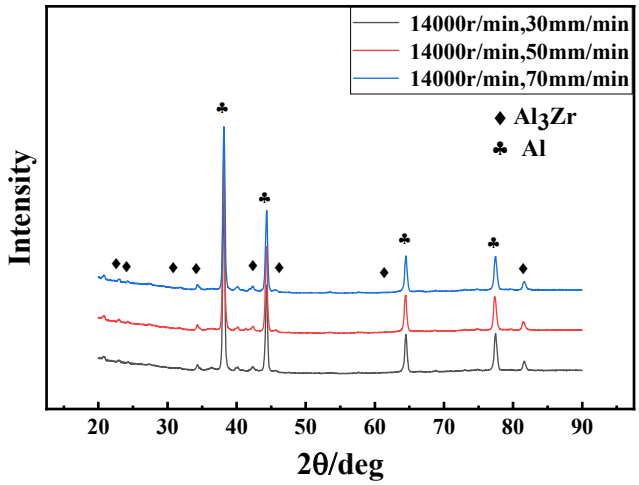

Fig. 8. XRD patterns of FSW joints with different welding parameters

Fig. 9 shows SEM micrograph of NZ of FSW joints under different welding parameters. It can be seen from the figure that the reinforcement particles in NZ of FSW joints were refined under various welding parameters. When the welding speed is 50 mm/min, the refinement effect is the best. When the welding speed is 70 mm/min, the weld NZ has obvious defects. The reinforcement particles of BM were aggregated, and the shape was mainly rectangular and few short rods, with the size of about 5-10 μm. The particle shape of well-distributed reinforced phase in NZ is mainly granular, with the size of about 1-5 μm. During FSW, the plasticized material was stirred by the stirring head. The reinforcement particles were extruded and broken under the shear force of the stirring pin, and evenly dispersed in the process of stirring and transportation. The fine and uniformly dispersed reinforcement particles bear most of the stress as nails, and hinder the movement of dislocations and the change of crystal boundary, which enhances the mechanical properties of the material.

In order to further analyze the influence of welding parameters on weld microstructure, the grain morphology of FSW joints with welding parameters of 14000 r/min and 50 mm/min is analyzed. Fig. 10(a) and 10(b) are the grain morphology of BM and HAZ of FSW joint. It can be seen that the grain size of HAZ is larger than that of BM. This is because compared with BM, HAZ is only affected by the welding thermal cycle without mechanical stirring, so only static recrystallization and the grain growth occurs. Fig. 10(c) and 10(d) are the advancing side and retreating side of FSW joint, respectively. It can be seen that the grain in NZ, whose shape is regular, is obviously smaller than that in BM and there is no large grain not broken. The interface between the weld zone and the base metal is relatively clear on the advancing side, while that is relatively vague on the retreating side. There is a small TMAZ region at the trailing edge of NZ, and the grains in the region are finer than those in HAZ. This is because the grains in the weld zone are fully broken by the stir-

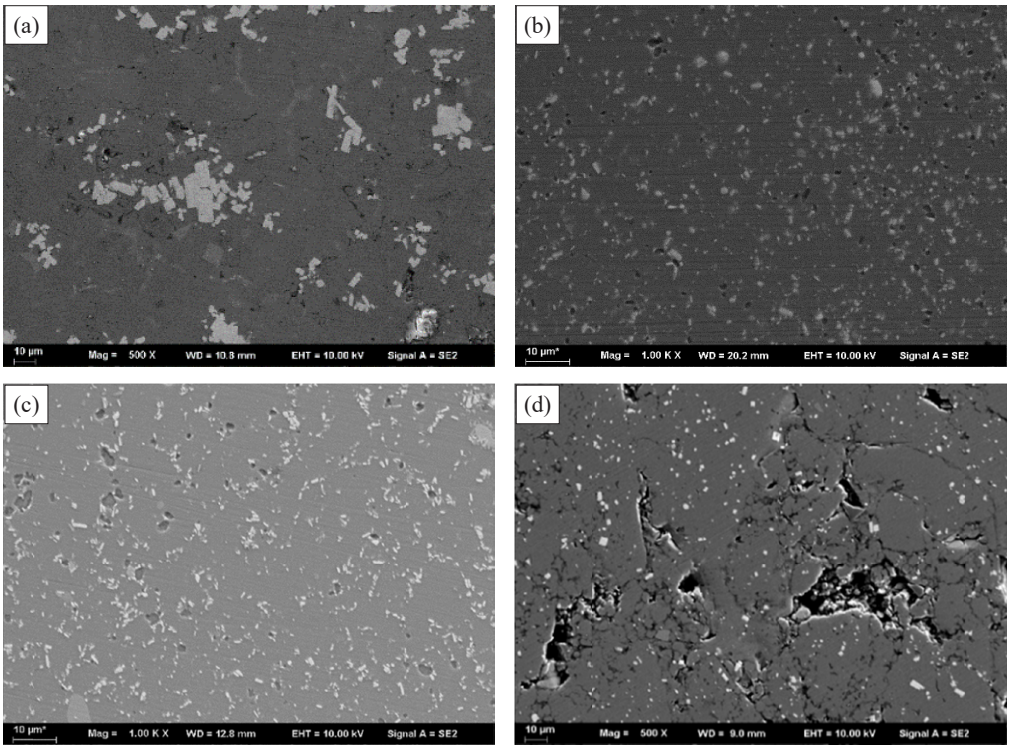

Fig. 9. SEM micrograph of NZ in FSW joints with different welding speeds. (a) BM; (b) 14000 r/min, 30 mm/min; (c) 14000 r/min, 50 mm/min; (d) 14000 r/min, 70 mm/min

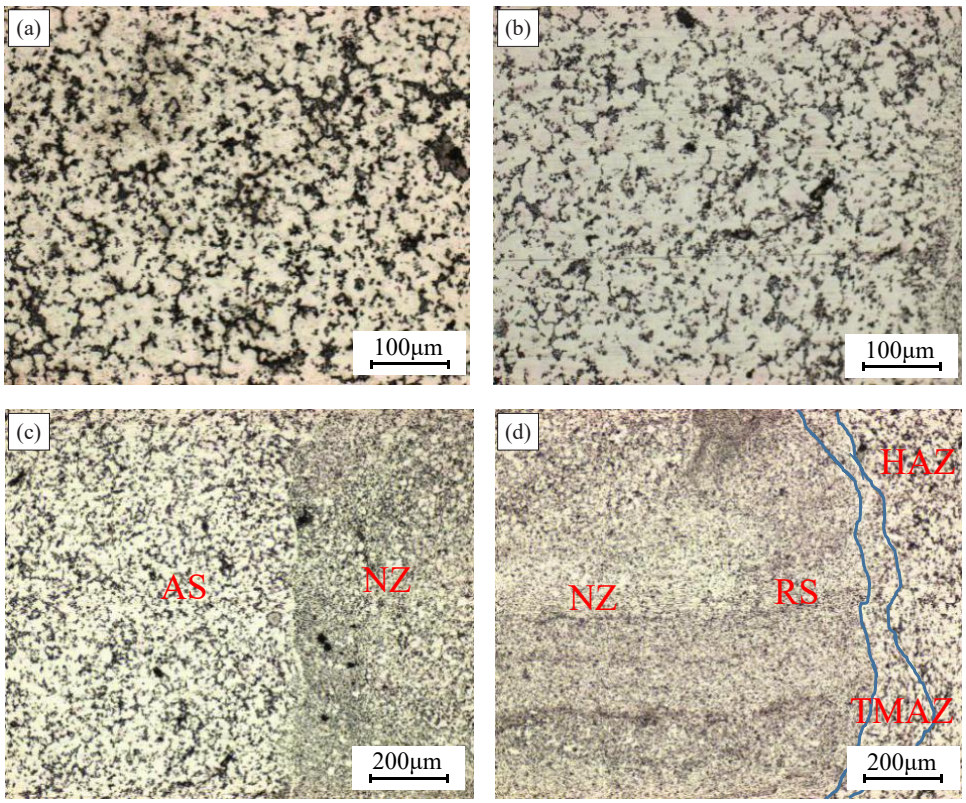

Fig. 10. Grain morphology of FSW joints with welding parameter of 14000 r/min, 50 mm/min. (a) BM; (b) HAZ; (c) AS; (d) RS

ring head and a large number of dislocations are accumulated in the microstructure due to great plastic deformation. In the process of entanglement and accumulation, these dislocations are connected into lines to form sub-crystal boundaries, which in turn leads to dynamic recrystallization in NZ, and the recrystallized grains are broken by the stirring head again. Thus, NZ is composed of equiaxed grains. However, the TMAZ region is located at the edge of the weld, with small area, low mechanical stirring and thermal cycle, so the recrystallized grains are not broken but elongated by the friction of the surrounding flow materials.

In order to further study the effect of friction stir welding process on weld microstructure, the weld of FSW joint of aluminum matrix composite sheet was observed by transmission electron microscope (TEM). The FSW joint weld with the welding parameters of 14000 r/min and 50 mm/min was selected as an example. Fig. 11 shows TEM microstructure of FSW joint.

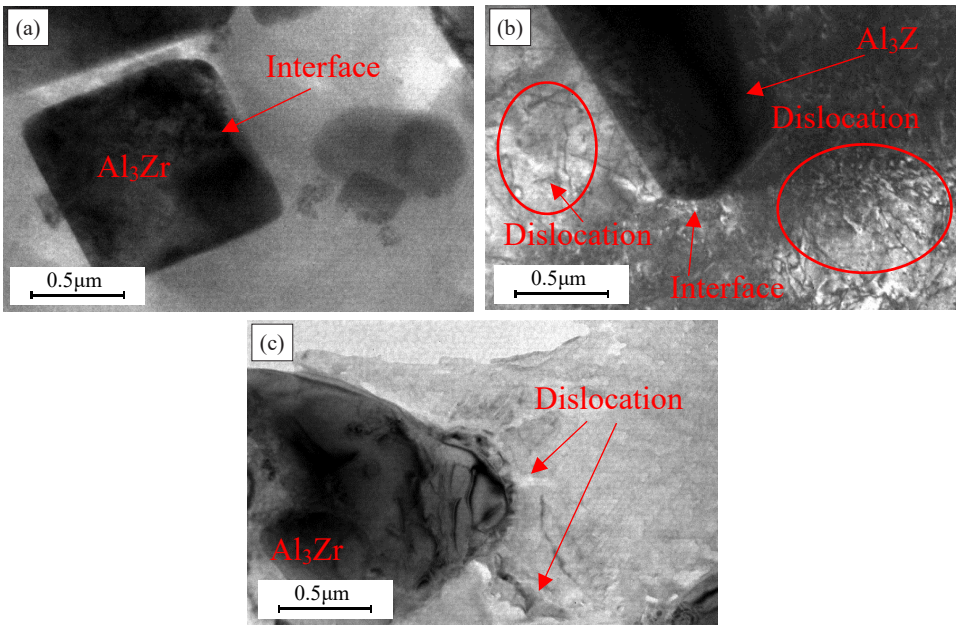

Fig. 11. TEM micrograph of FSW joint. (a) Reinforcing particles; (b-c) Interface between reinforcement particles and matrix

It can be found from the figure that there are reinforcement particles with a size of 1 μm in the weld microstructure, which indicates that the mechanical stirring of the stirring head fully breaks the reinforcement particles in the matrix. At the same time, there are a large number of dislocation tangles around the reinforcement particles, some of which are attached to the edge of the reinforcement particles. It can also be seen from the figure that the reinforcement particles in the weld microstructure and the edge of the matrix metal are clean, and there are no voids and other phases generated. This shows that when the aluminum matrix composites are subjected to severe stirring by the stirring head, the grains and the reinforcement particles are broken, and a large number of dislocations are generated in the matrix. A large number of dispersed reinforcement particles in the weld play a role of pinning, hindering the movement of dislocations and entangling a large number of dislocations around them to form dislocation walls. The existence of these dislocation tangles and dispersed reinforcement particles also strengthened the performance of FSW joint.

3.4. Texture analysis of FSW joints

In order to study the effect of different welding parameters on the microstructure of FSW joints, EBSD tests were performed on the joints with different welding parameters. Fig. 12 is the Inverse Pole Figure (IPF diagram) in NZ of FSW joint with different welding speeds. It can be seen from the diagram that the microstructure of FSW joints with various parameters presents disordered grain orientation distribution, which indicates that the microstructure at the weld is broken by the stirring head, resulting in disordered grain orientation and isotropic microstructure and properties. EBSD test results are similar to other related studies [32,36].

The weld microstructure of FSW joint with welding parameters of 14000 r/min and 50 mm/min was selected for characterization. Fig. 13 is the distribution of grain orientation difference in different regions of FSW joint. In the figure, the black line represents the High Angle Grain Boundaries (HAGBs) and the green line represents the Low Angle Grain Boundaries (LAGBs). It can be seen that the crystal boundaries in HAZ are sparse and mainly composed of HAGBs. On the contrary, the crystal boundaries in NZ are dense, which include many LAGBs. Fig. 14 shows the distribution of grain boundary orientation difference in different regions of FSW joint. It can be seen from the figure that the proportion of LAGB in HAZ is 24.35%, and that in NZ is 59.7%. NZ is subjected to intense mechanical stirring by the stirring head, so the grains are seriously deformed and broken, and the grains become fine, resulting in a large number of dislocations in the microstructure. However, when the grains reach the dynamic recrystallization temperature due to the welding thermal cycle, the fine reinforcement particles dispersed in NZ hinder the movement and fusion of dislocations, thus a large number of LAGBs are retained in NZ. HAZ is only affected by the welding thermal cycle, so a certain degree of static recrystallization occurs, the grains grow up and the dislocations in the microstructure decrease accordingly.

Fig. 15 shows the deformation characteristics of FSW joint with welding parameters of 14000 r/min, 50 mm/min. It can

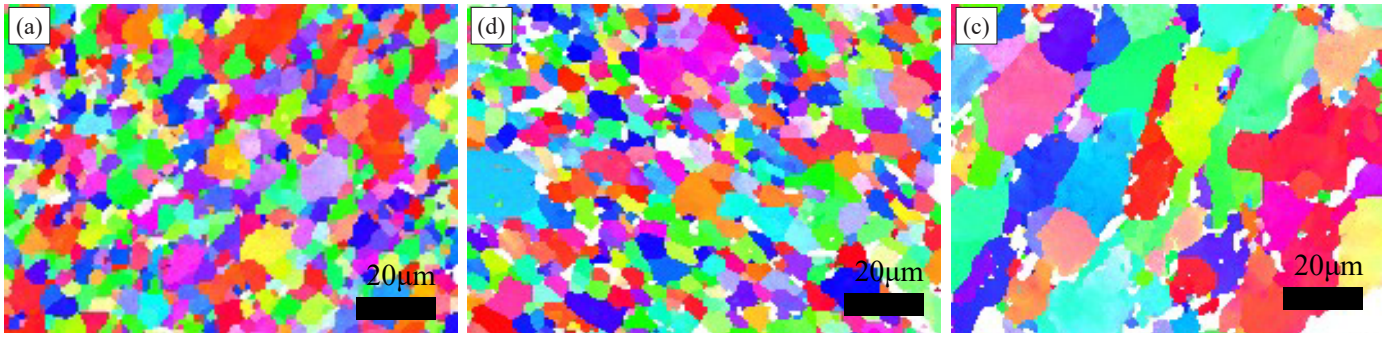

Fig. 12. IPF of NZ with different travel speeds. (a) 14000 r/min, 30 mm/min; (b) 14000 r/min, 50 mm/min; (c) 14000 r/min, 70 mm/min

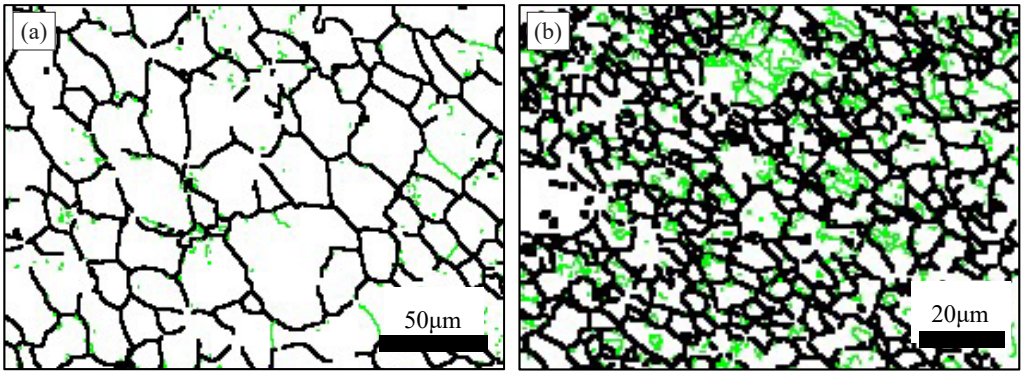

Fig. 13. Distribution of grain orientation difference in different regions of FSW joint. (a) HAZ; (b) NZ

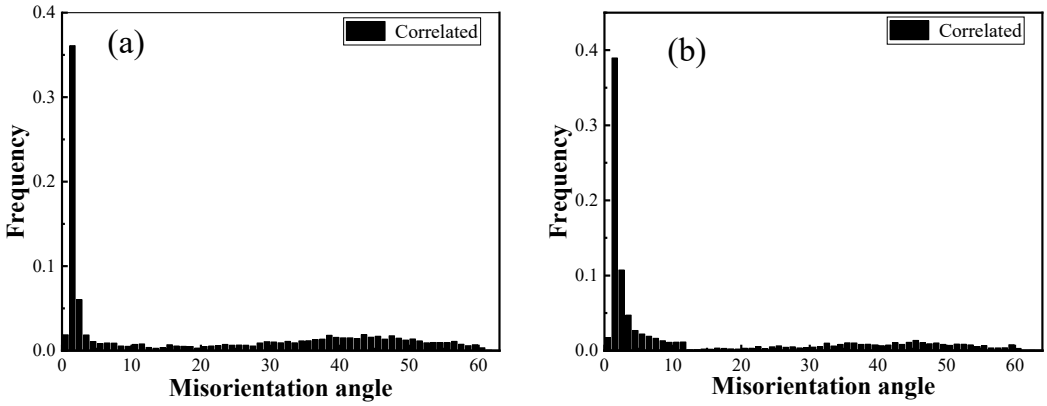

Fig. 14. Distribution of grain boundary orientation difference in different regions of FSW joint. (a) HAZ; (b) NZ

be seen from the diagram that the proportion of recrystallized microstructure in HAZ is higher, which is 37.18%, than the proportion of deformed microstructure, which is only 5.2%. The proportion of recrystallized microstructure in NZ is 23.65%, and that of deformed microstructure is 28.92%. There is only static recrystallization in HAZ, which is not mechanically stirred by the stirring head. So the recrystallization microstructure in HAZ is more than that in NZ, and the deformed microstructure in HAZ is very few. NZ is subjected to severe mechanical stirring, so the proportion of deformed microstructure in it is much higher than that in HAZ. At the same time, due to the block of reinforcement particles, there are no sufficient areas for dynamic recrystallization grains to grow. Thus, the proportion of recrystallization microstructure in NZ is lower than that in HAZ. This is consistent with the results of grain boundary orientation distribution in each region of the joint.

3.5. Mechanical properties of FSW joints

3.5.1. Microhardness of FSW joints

Fig. 16 shows the microhardness distribution of FSW joints with different welding parameters. It can be seen from the figure that the microhardness distribution of FSW joint section with welding parameters of 14000 r/min and 70 mm/min is arc, and

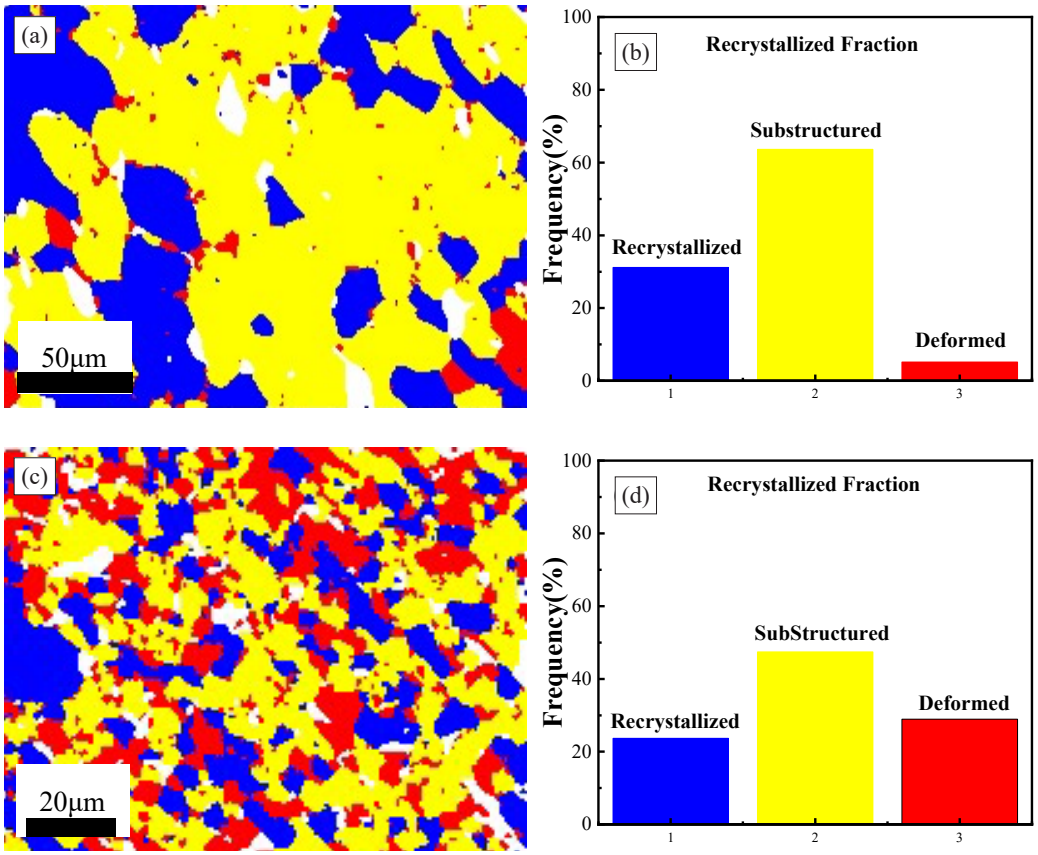

Fig. 15. Deformation characteristics of different regions of FSW joint. (a-b) HAZ; (c-d) NZ

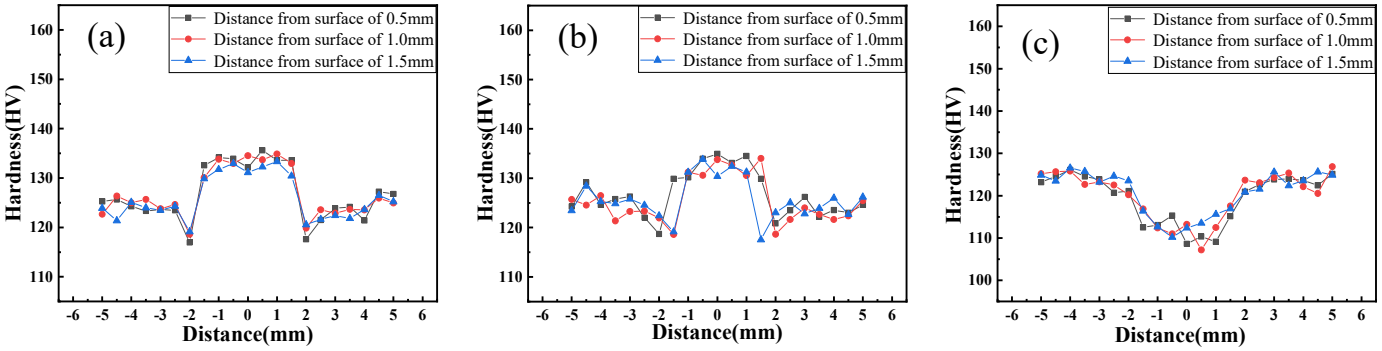

Fig. 16. Micro-hardness of FSW joints section with different process parameters. (a) 14000 r/min, 30 mm/min; (b) 14000 r/min, 50 mm/min; (c) 14000 r/min, 70 mm/min

the microhardness of the weld center area is slightly lower than that of the base metal area. This is because when the welding parameters are used, the welding thermal cycle effect on the weld zone is weak, and the degree of thermoplasticization of the material is low. The weld cannot be fully filled when the stirring pin is rotating, thereby making the weld microstructure not dense enough and reducing the microhardness at this place. The microhardness of FSW joints with other welding parameters shows 'W' type, that is, the microhardness of weld zone is the highest and that of HAZ is the lowest. The welding thermal cycle effect on FSW joints with the above welding parameters is relatively high. When the welding thermal cycle is high, the material at the weld can present a good thermoplastic state, and can be fully broken and transported to the rear gap when the stirring pin rotates. This makes the weld microstructure of FSW joint dense, the grain fine and the distribution of reinforcement particles dispersed. Because of this, mechanical properties are greatly improved. The higher welding thermal cycle makes the grains of HAZ recrystallization grow up, mechanical properties deteriorate and microhardness decrease. This indicates that the area of FSW joints,with the weakest mechanical properties, is HAZ. The results are consistent with the laws of relevant studies [37-39].

3.5.2. Tensile properties of FSW joints

Fig. 17 is the tensile curve of FSW joints with different welding speeds. It can be seen from the figure that the tensile strength and elongation of the tensile specimen of raw materials are the highest, which are 178(±0.5) MPa and 11.2%, respectively. When the rotating speed is 14000 r/min and the welding speed is 30, 50 and 70 mm/min, respectively, the tensile strength of FSW joint is 132(±0.5), 142(±0.5) and 77(±0.5) MPa, and the elongation is 8.4%, 8.2% and 6.3%. The tensile strength of FSW joint with welding speed of 50 mm/min is the highest; the tensile strength of FSW joint with welding speed of 30 mm/min is slightly lower; and the tensile strength of FSW joint with welding speed of 70 mm/min is the lowest. The fracture strain of FSW joint with welding speed of 30 mm/min is slightly higher than that of joint with welding speed of 50 mm/min. This is because different welding heat inputs have a great impact on the microstructure and properties of FSW joints. When the welding speed is fixed, the friction heat generated by the stirring head and the shoulder in unit time is fixed. The higher the welding speed is, the lower the welding thermal cycle of the weld in unit time is, and the lower the plasticizing degree of the material is. It is more difficult for the stirring head to transport the material to the rear vacancy, which makes the weld microstructure have a large number of holes and other defects, and the weld center becomes a region with poor performance. Therefore, the tensile strength of the FSW joint with the welding speed of 70 mm/min is the lowest. When the welding speed is 30 mm/min, the welding thermal cycle of the weld is higher than that of the FSW joint with the welding speed of 50 mm/min, so the plasticizing degree of the material is the highest and the weld microstructure is dense. However, due to the large amount of welding heat input, the grain growth in HAZ leads to the decrease of the mechanical properties of FSW joints. Therefore, the tensile strength of this FSW joint is slightly lower than that of FSW joint with welding speed of 50 mm/min.

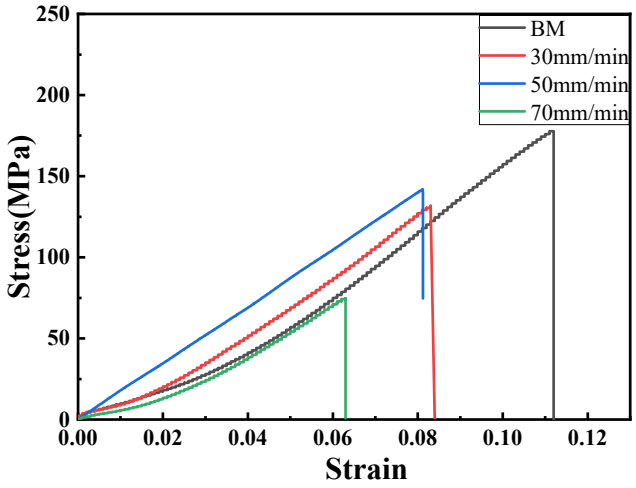

Fig. 17. Tensile curves of FSW joints with different welding speeds

Fig. 18(a-f) is the tensile fracture morphology of FSW joints with different welding speeds. The fracture of FSW joint with welding speed of 70 mm/min is in the weld, and there is a large

area of hole surface can be seen, which shows that there are a lot of defects in the weld microstructure at the fracture. The dimples on the fracture surface are large and shallow, and there are a large number of reinforcement particles on the dimple surface. When the welding speed is reduced to 30 mm/min, the fracture of FSW joint is in HAZ, and the dimple at the fracture is larger and deeper than that of the joint with 50 mm/min welding speed. This is because when the welding speed is fixed, the welding heat input is also fixed. With the increase of the welding speed, the welding thermal cycle of the material at the weld in unit time decreases. Therefore, when the welding speed is 70 mm/min, the plasticizing degree of metal materials at the weld is poor, and the material cannot be fully filled by the stirring head, which makes the weld have a lot of defects such as holes. These defects greatly reduce the mechanical properties of the joints, and the tensile fracture occurs preferentially at the defects. At the same time, due to the failure of the stirring head to fully stir the weld material, the reinforcement particles in this place have gathered to a certain extent. These reinforcement particles bear most of the tensile stress and become the stress-concentration points. When the stress exceeds the combination strength of the matrix and reinforcement, the fracture occurs. The dimple size at the fracture is small and the depth is shallow. When the welding speed is 30 mm/min, the plasticizing degree of the material at the weld is the highest, and the weld microstructure is the most dense, so the fracture is in HAZ with the worst performance. The welding thermal cycle of HAZ of the FSW joint is the highest, so the static recrystallization of grains is more obvious and the grain grows larger, which makes the dimple size of the fracture in HAZ larger. The fracture morphology and mechanism accord with the general law of aluminum matrix composites [36,40].

4. Conclusions

In order to explore the ultra-high rotating speed friction stir welding performance of aluminum matrix composite sheet and the possibility of its industrial application, the effects of different

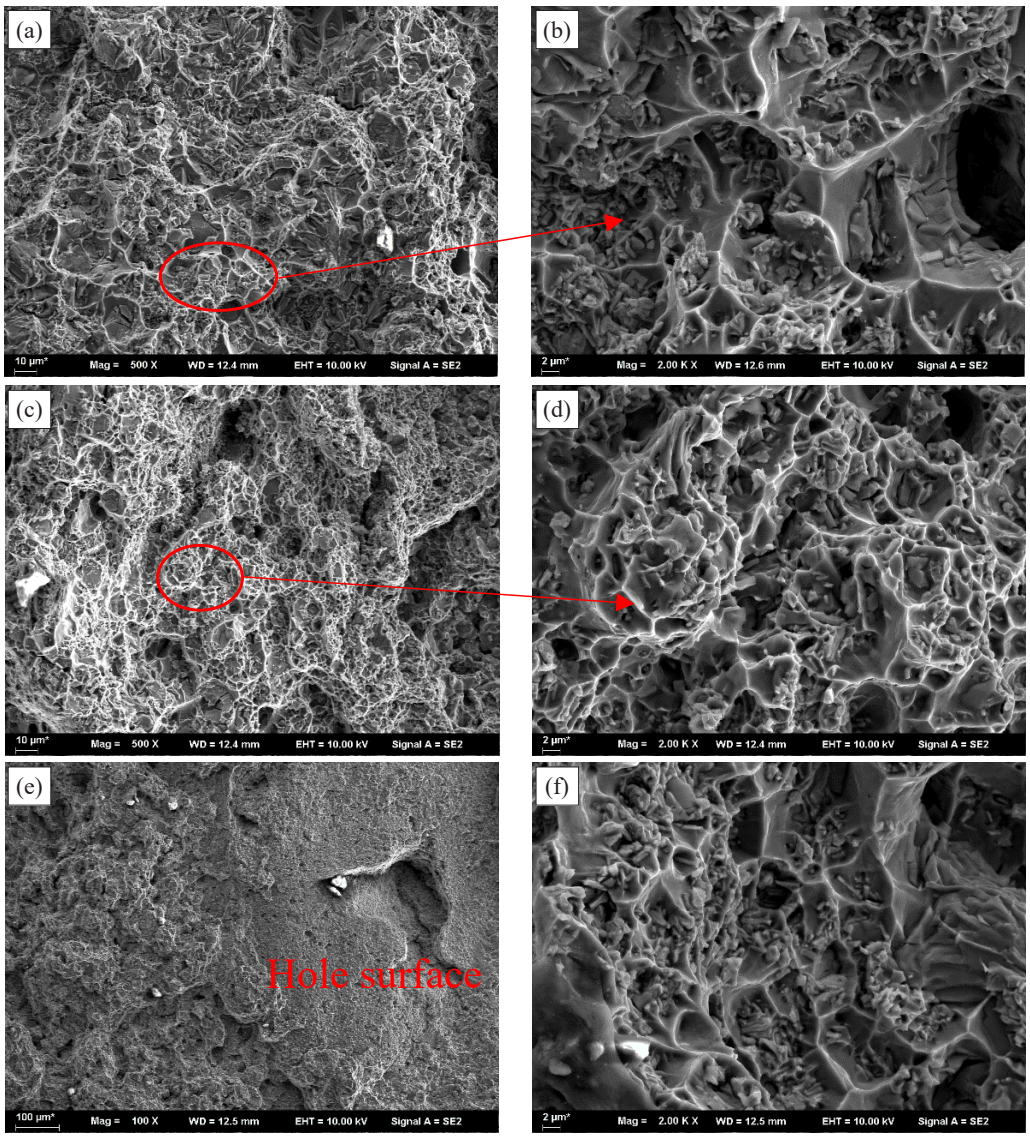

Fig. 18. Tensile fracture morphology of FSW joints with different welding parameters. (a-b) 14000 r/min, 30 mm/min; (c-d) 14000 r/min, 50 mm/min; (e-f) 14000 r/min, 70 mm/min

welding speeds on the microstructure and mechanical properties of FSW joints of 2 mm sheet were studied at the rotating speed of 14000 r/min.

(1) When the welding speed is high, the weld is prone to defects such as holes. When the welding speed is low, the weld surface is prone to overburn, and the edge is prone to flash. The FSW joint with welding speed of 50 mm/min has the best weld formation.

(2) No new phases were produced in FSW joints with different welding parameters. The refining effect of stirring pin on the grains and reinforcement particles in the weld zone is obvious, while the grains grow up in the HAZ due to static recrystallization. The reinforcement particles in the weld microstructure are well bonded to the matrix and dislocation entanglement occurs nearby. With the increase of welding speed, the weld width decreases.

(3) The microstructure of FSW joint with welding speed of 70 mm/min is poor, and there are a lot of holes and other defects.The microhardness of NZ in the weld section is lower than that of BM. In all tensile tests, the fractures occurred in the center of the weld. The microhardness of FSW joints with other welding parameters is 'W' type, that is, the microhardness of NZ is the highest and that of HAZ is the lowest. The FSW joint with welding speed of 50 mm/min has the best tensile strength of 142(±0.5) MPa and elongation of 8.2%. The FSW joint with welding speed of 30 mm/min has the maximum fracture strain of 0.084.

(4) There is no texture in FSW joints and grain orientation is disordered. The proportion of LAGB in NZ of FSW joint with welding speed of 50 mm/min is 59.7%, and the proportion of recrystallized grain structure is 23.65%. The proportion of LAGB in HAZ is 24.35%, and the proportion of recrystallized grain structure is 37.18%.

Acknowledgement

(1) This research was financially supported by the National Natural Science Foundation of China, No. 51605206.

(2) Postgraduate Research & practice Inovation Program of Jiangsu Province, No.SJCX 21_1769.

(3) Jiangsu Province key Laboratory of High-end structural Materials, No.hsm1806.

REFERENCE

[1] A. Hadadzadeh, M. M. Ghaznavi, A. H. Kokabi, HAZ softening behavior of strain hardened A1-6.7Mg alloy welded by GMAW and pulsed GMAW processes, The International Journal of Advanced Manufacturing Technology **92** (5-8), 2255-2265 (2017). DOI: https://doi.org/10.1007/s00170-017-0318-x

[2] G.Q. Chen, J.B. Liu, X. Shu, Research progress and analysis of aluminum alloy welding, Welding & Joining (09), **7**, 12-68 (2017).

[3] A. Amini, P. Asadi, P. Zolghadr, Friction stir welding applications in industry. Advances in friction stir welding and processing, 2014 Woodhead.

[4] H. Li, P.Y. Xu, Y.P. Qiao, Microstructure and Mechanical Properties of Ultrahigh-Speed Friction-Stir-Welded Joints of In Situ Al_3Zr Particle-Reinforced Aluminum Matrix Composite Sheets. Adv. Eng. Mater. **23** (8), 2100295 (2021). DOI: https://doi.org/10.1002/adem.202100295

[5] G.K. Padhy, C.S. Wu, S. Gao, Friction stir based welding and processing technologies-processes, parameters, microstructures and applications: A review, J. Mater. Sci. Technol. **34**, 1-38 (2018). DOI: https://doi.org/10.1016/j.jmst.2017.11.029

[6] P. Prakash, S.K. Jha, S.P. Lal, Numerical investigation of stirred zone shape and its effect on mechanical properties in friction stir welding process, Welding World. **63**, 1531-1546 (2019). DOI: https://doi.org/10.1007/s40194-019-00787-0

[7] A.R. Rose, K. Manisekar, V. Balasubramanian, Effect of axial force on microstructure and tensile properties of friction stir welded AZ61A magnesium alloy, Transactions of Nonferrous Metals Society of China. **21** (5), 974-984 (2011). DOI: https://doi.org/10.1016/s1003-6326(11)60809-1

[8] X.J. Wang, L. Feng, J.T. Wu, X.H. Xiao, B.B. Su, Study of Bending Strength and Fracture Behavior of ZK60 Mg Alloy Welded by Friction Stir Welding, Materials Reports **34** (04), 4083-4086 (2020).

[9] Q.S. Ma, Y.J. Li, J. Wang, Microstructure characteristic and shear strength of wideband laser clad Ni60 composite coatings reinforced with WC particle, Transactions of the China Welding Institution **37** (12), 49-52+131 (2016).

[10]G. Cam, S. Mistikoglu, Recent Developments in Friction Stir Welding of Al-alloys, Journal of Materials Engineering & Performance **23** (6), 1936-1953 (2014). DOI: https://doi.org/10.1007/s11665-014-0968-x

[11] O.S. Salih, H. Ou, W. Sun, D.G. McCartney, A review of friction stir welding of aluminium matrix composites, Mater. Des. **86**, 61-71 (2015). DOI: https://doi.org/10.1016/j.matdes.2015.07.071

[12] L. Jiao, F. Li, Y.T. Zhao, Microstructure and tribological behavior of in situ ZrB_2/A356 composites prepared under magnetic field, Surf. Topogr.: Metrol. Prop. **9** (1), 015026 (2021). DOI: https://doi.org/10.1088/2051-672X/abe720

[13] S.Y. Yang, H.R. Zhong, Y.S. Tao, Microstructure and Properties of Friction Stir Welded Joints of Magnesium Rare Earth Alloy, Chinese Journal of Rare Metals **37** (01), 33-37 (2013).

[14] H.Y. Zhou. Research on the Friction Stir Welding of Al/Mg Dissmillar Alloy. Master's thesis. Nanjing University of Science & Technology, Nanjing, Jiangsu, June.

[15] Roosvel Soto-Díaz, Anderson Sandoval-Amador, Jimy Unfried-Silgado, The International Journal of Advanced Manufacturing Technology (2021). DOI: https://doi.org/10.1007/s00170-021-07373-z (in press).

[16] S.D. Ji, Q. Wen, L. Ma, Microstructure along thickness direction of fricyion stir welded TC4 titanium alloy joint, Acta Metallurgica Sinica **51** (11), 1391-1399 (2015).

[17] H. Li, P.Y. Xu, L. Jiao, Surface wear behavior and strengthening mechanism of Al3Zr particle reinforced aluminum matrix com-

posites prepared in situ, Surf. Topogr.: Metrol. Prop. **7** (4), 045013 (2019). DOI: https://doi.org/10.1088/2051-672X/ab4145

[18] Y.H. Sun, L. Du, Development and Application of Friction Stir Welding, New Technology & New Process (06), 70-73 (2011).

[19] S. Ji, Y. Wang, Z. Li, Effect of Plate Thickness on Tensile Property of Ti-6Al-4V Alloy Joint Friction Stir Welded Below β-Transus Temperature, High Temperature Materials and Processes **36** (7), 693-699 (2017). DOI: https://doi.org/10.1515/htmp-2016-0012

[20] G. Çam, G. İpekoğlu, Recent developments in joining of aluminum alloys, Int. J. Adv. Manuf. Technol. **91**, 1851-1866 (2017). DOI: https://doi.org/10.1007/s00170-016-9861-0

[21] A. Sasikumar, S. Gopi, G. Mohan Dhanesh, Effect of welding speed on mechanical properties and corrosion resistance rates of filler induced friction stir welded AA6082 and AA5052 joints, Materials Research Express **8** (6), 066531 (2021). DOI: https://doi.org/10.1088/2053-1591/AC0C9E

[22] L. Jiao, F. Li, Y.T. Zhao, Surface Friction and Wear Behavior of In Situ AlB_2 Particle-Reinforced A356 Composites, J. of Materi Eng and Perform. (2022). DOI: https://doi.org/10.1007/s11665-022-06626-6

[23] Hassan Khairia Salman, Abbass Muna Khethier, Mohammed Mohsin Talib, Effect of Surface Finishing on Microstructure and Corrosion Behavior of Friction Stir Welded Joints For Dissimilar Aluminum Alloys (AA2024-T3 with AA6061-T6), IOP Conference Series: Materials Science and Engineering 1105 (1), 012047 (2021). DOI: https://doi.org/10.1088/1757-899x/1105/1/012047

[24] S. Mironov, T. Onuma, Y.S. Sato, Microstructure evolution during friction stir welding of AZ31 magnesium alloy, Acta Materialia **100**, 301-312 (2015). DOI: https://doi.org/10.1016/j.actamat.2015.08.066

[25] W.F. Xu, J.H. Liu, D.L. Chen, Influence of Test Temperature on the Tensile Properties along the Thickness in a Friction Stir Welded Aluminum Alloy, Journal of Materials Science & Technology **31** (9), 953-961 (2015). DOI: https://doi.org/10.1016/j.jmst.2015.07.005

[26] N. Kashaev, V. Ventzke, G. Çam, Prospects of laser beam welding and friction stir welding processes for aluminum airframe structural applications, J. Manuf. Processes **36**, 571-600 (2018). DOI: https://doi.org/10.1016/j.jmapro.2018.10.005

[27] P. Prabhuraj, S. Rajakumar, Experimental investigation on corrosion behavior of friction stir welded AA7075-T651 aluminium alloy under 3.5% wt NaCl environment, Materials Today: Proceedings **45**, 5878-5885 (2021). DOI: https://doi.org/10.1016/j.matpr.2020.08.422

[28] H. Li, Y.P. Qiao, S.B. Lu, J. of Mater. Eng. and Perform. (2022), DOI: https://doi.org/10.1007/s11665-022-06652-4 (in press).

[29] R. Ye, J.D. Yang, X.Y. Peng, Microstructure, mechanical properties and localized corrosion property of friction stir welded joint of Al-Zn-Mg-Sc-Zr alloy, The Chinese Journal of Nonferrous Metals **25** (10), 2656-2665 (2015).

[30] J. Zhang, P. Upadhyay, Y. Hovanski, D.P. Field, High-speed friction stir welding of AA7075-T6 sheet: microstructure, mechanical properties, micro-texture, and thermal history, Metall. Mater. Trans. A. **49**, 210-222 (2018). DOI: https://doi.org/10.1007/s11661-017-4411-4

[31] C. Gao, Z. Zhu, J. Han, H. Li, Correlation of microstructure and mechanical properties in friction stir welded 2198-T8 Al-Li alloy, Mater. Sci. Eng. A. **639**, 489-499 (2015). DOI: https://doi.org/10.1016/j.msea.2015.05.038

[32] C. Yang, J.F. Zhang, G.N. Ma, Microstructure and mechanical properties of double-side friction stir welded 6082Al ultra-thick plates, Journal of Materials Science & Technology **41**, 105-116 (2020). DOI: https://doi.org/10.1016/j.jmst.2019.10.005

[33] L.Z. Zhao, M. Yang, Study on particle reinforced aluminum matrix composites, Hot Working Technology.. **40** (20), 107-110 (2011). DOI: https://doi.org/10.3969/j.issn.1001-3814.2011.20.033

[34] J. Hashim, L. Looney, M.S.J. Hashni,The Wettability of SiC Particles by Molten Aluminium Alloy, J. Mater. Processing Tech. **119**, 324-328 (2001). DOI: https://doi.org/10.1016/s0924-0136(01)00975-x

[35] S. Rajkumar, K. Mageshkumar, K. Arul, Materials Today: Proceedings. (2022). DOI: https://doi.org/10.1016/j.matpr.2022.01.473 (in press).

[36] T. Ding, H.G. Yan, J.H. Chen, Effect of welding speed on microstructure and mechanical properties of Al−Mg−Mn−Zr−Ti alloy sheet during friction stir welding, Trans. Nonferrous Met. Soc. China **31**, 3626-3642 (2021). DOI: https://doi.org/10.1016/S1003-6326(21)65753-9

[37] Ravi Kumar, A. Nait Salah, Neeraj Kant, Effect of FSW process parameters on mechanical properties and microstructure of dissimilar welded joints of AA2024 and AA6082, Materials Today: Proceedings **50**, 1435-1441 (2022). DOI: https://doi.org/10.1016/j.matpr.2021.09.007

[38] I. Vysotskii, S. Malopheyev, S. Mironov, R. Kaibyshev, Deformation behavior of friction-stir welded Al-Mg-Mn alloy with ultrafine-grained structure, Materials Characterization **185**, 111758 (2022). DOI: https://doi.org/10.1016/j.matchar.2022.111758

[39] K. Krasnowski, C. Hamilton, S. Dymek, Influence of the tool shape and weld configuration on microstructure and mechanical properties of the Al 6082 alloy FSW joints, Archives of Civil and Mechanical Engineering **15** (1), 133-141 (2015). DOI: https://doi.org/10.1016/j.acme.2014.02.001

[40] C.C. Dua, X. Wang, Q.H. Pan, SVET, Correlation between microstructure and mechanical properties of 6061-T6 double-side FSW joint, Journal of Manufacturing Processes **38**, 122-134 (2019). DOI: https://doi.org/10.1016/j.jmapro.2019.01.010